PHYSICAL REVIEW A **91**, 061403(R) (2015)

Dressing effects in the attosecond transient absorption spectra of doubly excited states in helium

L. Argenti,[1,*] Á. Jiménez-Galán,[1] C. Marante,[1] C. Ott,[2] T. Pfeifer,[2,3] and F. Martín[1,4,5]

[1]*Departamento de Química, Módulo 13, Universidad Autónoma de Madrid, 28049 Madrid, Spain, EU*

[2]*Max-Planck Institut für Kernphysik, Saupfercheckweg 1, 69117 Heidelberg, Germany, EU*

[3]*Center for Quantum Dynamics, Ruprecht-Karls-Universität Heidelberg, 69120 Heidelberg, Germany, EU*

[4]*Instituto Madrileño de Estudios Avanzados en Nanociencia (IMDEA-Nanociencia), Cantoblanco, 28049 Madrid, Spain, EU*

[5]*Condensed Matter Physics Center (IFIMAC), Universidad Autónoma de Madrid, 28049 Madrid, Spain, EU*

(Received 18 February 2015; published 11 June 2015)

Strong-field manipulation of autoionizing states is a crucial aspect of electronic quantum control. Recent measurements of the attosecond transient absorption spectrum (ATAS) of helium dressed by a few-cycle visible pulse [C. Ott *et al.*, Nature (London) **516**, 374 (2014)] provide evidence of the inversion of Fano profiles. With the support of accurate *ab initio* calculations that reproduce the results of the latter experiment, here we investigate the new physics that arise from ATAS when the laser intensity is increased. In particular, we show that (i) previously unnoticed signatures of the dark $2p^2\,{}^1S$ doubly excited state are observed in the experimental spectrum, (ii) inversion of Fano profiles is predicted to be periodic in the laser intensity, and (iii) the ac Stark shift of the higher terms in the $sp^+_{2,n}$ autoionizing series exceeds the ponderomotive energy, which is the result of a genuine two-electron contribution to the polarization of the excited atom.

DOI: 10.1103/PhysRevA.91.061403 PACS number(s): 32.80.Qk, 32.80.Fb, 32.80.Rm, 32.80.Zb

I. INTRODUCTION

Attosecond laser pulses give access to the time-resolved motion of correlated electron dynamics in atoms, molecules, and solids on their natural time scale [1]. In this context, attosecond transient absorption spectroscopy (ATAS) [2–4] has affirmed itself as a valid technique to monitor and control electronic wave packets [2,5,6]. For example, it has been used to demonstrate hole alignment in neon [7], to track the field-free ultrafast dynamics of coherent ensembles of valence-hole excited states in krypton [2,8], of singly excited bound states in neon [6,9] and helium [10–14], and of doubly excited states in helium [5]. Compared to photofragment detection [15,16], ATAS provides easier access to higher energy resolution. Furthermore, while photoelectron distributions are asymptotic properties, and thus often complicate the analysis due to long-range Coulomb interaction effects, the calculation of ATAS spectra only requires the electronic wave function in the vicinity of the reaction center.

Electronic wave packets can be controlled by altering the relative phase of their components, e.g., with a short light pulse that imparts a temporary intensity-dependent ac Stark shift $\Delta E^{\rm ac}(I)$ on the states it is composed of. The corresponding phase excursion, $\Delta\phi_i = \int dt\, \Delta E_i^{\rm ac}[I(t)]/\hbar$, maps onto the modulation of the asymmetry of the resonant profiles in the ATAS spectrum [17–19]. This principle has been recently applied to a metastable two-electron wave packet in the helium atom, formed by the $sp^+_{2,n}\,{}^1P^o$ doubly excited states (DES) [5,17]. The experiment evidenced also the Autler-Townes (AT) splitting of the $sp^+_{2,2}$ state, which is coupled to the $2p^2\,{}^1S$ state [5], as well as inversion of the Fano profile in the higher terms of the $sp^+_{2,n}$ series as a function of both the time delay between the extreme ultraviolet (XUV) and the VIS pulses, and the intensity of the VIS dressing field [17].

Here we show, by means of accurate *ab initio* calculations that reproduce the experimental results for the helium atom, that ATAS in the XUV around 60 eV can be used to obtain information on strongly correlated electrons dressed by a few-cycle moderately intense visible (VIS) pulse ($\mathrm{FWHM}_{\rm VIS} = 7$ fs, $\lambda_{\rm VIS} = 730$ nm). In particular, we highlight clear signatures of the supposedly dark $2p^2\,{}^1S$ state in the spectrum, and of two-photon absorption above the $N = 2$ threshold, from the $sp^+_{2,3-5}\,{}^1P^o$ autoionizing states. By increasing the VIS intensity beyond the values used in the experiment, we unambiguously show that the ac Stark shift of these latter peaks is larger than the ponderomotive energy. This circumstance indicates that the concurrent motion of the two correlated electrons plays a crucial role in the response of the electron wave packet to the driving laser field at relatively high intensities. Furthermore, we predict that the inversion of the Fano profile observed in the experiment by increasing the laser intensity, actually repeats itself multiple times as the intensity is increased even further, before the resonant signals in the spectrum eventually disappear. Finally, we interpret the ATAS spectrum in terms of the nondiagonal XUV effective linear susceptibility of the dressed atom, which is the basis for bidimensional spectroscopy in the XUV energy range.

II. COMPUTATION OF THE ATAS SPECTRUM

In ATAS, the weak XUV pulse $\mathcal{E}(t)$ induces a time-dependent dipole moment $d(t;\mathcal{E})$ in the atom dressed by the VIS field. In turn, the dipole gives rise to an emission that interferes with the field and alters the spectrum of the XUV transmitted pulse (see Fig. 1). For an optically thin medium, the relative change of the spectral intensity of the XUV pulse can be expressed in terms of an effective transient-absorption atomic cross section [20] (atomic units, a.u., are used unless otherwise indicated),

$$\sigma(\omega;\tilde{\mathcal{E}}) = 4\pi\alpha\omega\,\mathrm{Im}[\tilde{d}(\omega;\tilde{\mathcal{E}})/\tilde{\mathcal{E}}(\omega)], \qquad (1)$$

*luca.argenti@uam.es

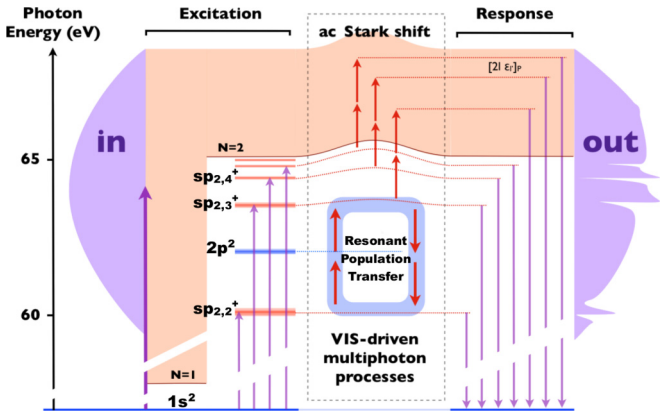

FIG. 1. (Color online) Energy level scheme. The ATAS of helium records the linear response in the XUV energy range of the atom dressed by an external VIS field. The attosecond XUV pulse excites a wide range of continuum and DES states (left) whose population and phase are altered by the dressing laser, due to multiphoton and nonperturbative transitions (center). The dipole response of the atom (right) reflects such change.

where $\tilde{d}$ and $\tilde{\mathcal{E}}$ are the Fourier transform (FT) of the component of the dipole moment and the XUV field along the laser polarization, respectively, while $\alpha = e^2/\hbar c$ is the fine-structure constant. Common analytical strong-field ionization models [21–28] are based on the single-active-electron (SAE) approximation, on the adiabatic approximations, and neglect the dynamic polarizability of the parent ion [29,30]. Therefore, they are of limited value for the strongly correlated DES of helium. The short duration of the dressing pulses in ATAS, furthermore, limits the pertinence of *ab initio* studies conducted in stationary regimes as well [20,31–33]. Quantitative interpretation of these experiments requires instead both a complete *ab initio* representation of the system and a direct solution of the time-dependent Schrödinger equation (TDSE).

Here, we solve the TDSE with a second-order exponential time-step propagator in velocity gauge [34,35]. Reflection from the box boundaries is prevented by complex absorbing potentials. The wave function is expanded on a two-particle spherical basis: the angular part is represented by bipolar spherical harmonics [36] and the radial part by B splines. Each total angular momentum comprises all the partial-wave channels with configurations $N\ell\epsilon_{\ell'}$ with $N \leqslant 2$ and $\ell' \leqslant 11$, and full-CI localized channels $n\ell n'\ell'$ ($\ell,\ell' < 5$) that reproduce short-range correlations between the two electrons [37] (see methods in [5]). The TDSE solver is implemented in a parallel program based on the PETSC libraries [38–40]. The ATAS response is evaluated with a velocity-gauge analog of Eq. (1) obtained via the Ehrenfest theorem,

$$\sigma(\omega;\tilde{A}) = -4\pi\omega^{-1}\,\mathrm{Im}[\tilde{p}(\omega;\tilde{A})/\tilde{A}(\omega)], \qquad (2)$$

where $\tilde{A}$ and $\tilde{p}$ are the Fourier transform of the vector potential and of the canonical momentum, respectively. The momentum $\tilde{p}$ is given by the sum of two complementary terms: $\tilde{p}_-$, computed numerically while in the presence of the dressing field; and $\tilde{p}_+$, computed analytically for the subsequent field-free evolution. The result is thus equivalent to the one that would be obtained for a simulation protracted for an infinite time.

III. COMPARISON WITH THE EXPERIMENT

In Fig. 2 we compare the present theoretical ATAS spectrum $\sigma(\omega;\tau)$, as a function of the photon energy and the time delay τ, to the experimentally measured optical density (OD) [17] (OD $\propto \sigma$) for theoretical and experimental laser intensities $I_0^{\mathrm{th}} = 3.5$ TW/cm^2 and $I_0^{\mathrm{expt.}} = 3.3 \pm 1.5$ TW/cm^2, respectively. The agreement is excellent. The vertical features visible in the two spectra are due to the bright $sp^+_{2,n}$ series of doubly excited states, $n = 2, 3, \ldots$ [41]. At large negative time delays, when the dressing pulse arrives well before the XUV pulse, the ATAS spectrum displays the characteristic Fano profiles of the field-free atom [41–43]. When the two pulses overlap, the $sp^+_{2,2}$ state separates into two AT branches, associated with the well-known coupling between the $sp^+_{2,2}$ and the $2p^2\,{}^1S$ state [17,26,32]. With the current energy of the dressing field, $\hbar\omega_{\mathrm{VIS}} = 1.7$ eV, the latter is resonantly coupled to both the first and the second term of the $sp^+_{2,n}$ series [35] (see Fig. 1). On account of its even parity, the $2p^2\,{}^1S$ is normally a "dark" state. Yet, due to the mixing with the ${}^1P^o$ DES promoted by the VIS pulse, the dipole amplitude between the dressed $2p^2\,{}^1S$ state and the ground state is actually not zero. The clear signatures of the upper AT branch in both the theoretical and the experimental spectra close to the $2p^2\,{}^1S$ state, shown in the insets of Fig. 2 with enhanced

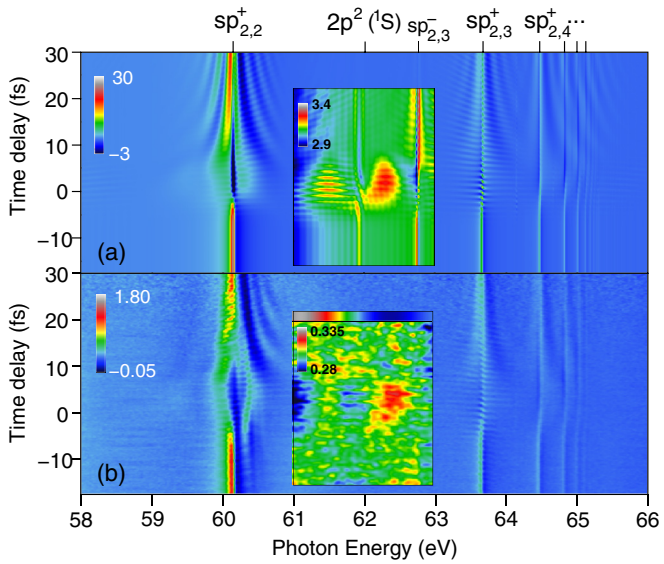

FIG. 2. (Color online) (a) Theoretical ATAS spectrum as a function of the XUV photon energy (x axis) and of the VIS-XUV time delay (y axis), for $I_{\mathrm{VIS}} = 3.5$ TW/cm^2. (b) Experimental spectrum recorded for $I_{\mathrm{VIS}} = 3.3 \pm 1.5$ TW/cm^2. In the insets, closer inspection unveils signatures of the $2p^2\,{}^1S$ resonance. In the experimental spectrum, the faint feature of the $2p^2$ "dark" state appears as a shoulder on a background, of instrumental origin, that varies steeply along the energy axis. To better highlight the resonance, therefore, in the inset of the lower panel we subtracted the variable part of the background, obtained from a polynomial fit and shown in color along the frame upper edge.

contrast, confirm this expectation. At very large time delays, the signal converges again to the field-free case. Here, the fringes converging around each resonance are a consequence of the sharp change in the phase and population of the localized part of the resonances induced by the strong VIS pulse and can thus be seen as experimental evidence of the formation of a Fano profile in the continuum [44] (the fringes on the higher-energy side of the resonance have better contrast due to the smaller slope of the asymmetric-peak background in this spectral region). In the dark narrow region between the two AT branches of the $sp^+_{2,2}$ state, the effective transient absorption cross section is negative, i.e., the XUV field is amplified rather than absorbed. This observation confirms previous predictions [4,20,26] and experimental findings [8,23]. The faint transversal hyperbolic fringes visible on top of the $sp^+_{2,2}$ and $sp^+_{2,3}$ terms for positive time delays, $\tau_n(E) = 2\pi n/|E - E_{sp^+_{2,3/2}}|$, respectively, arise from the interference between the direct one-photon excitation amplitude from the ground state, $\mathcal{A}_{sp^+_{2,2/3}\leftarrow g}$, and the resonantly enhanced two-VIS-photon emission and absorption amplitude from the other XUV-excited autoionizing state $\mathcal{A}_{sp^+_{2,2/3}\leftarrow[2p^2]\leftarrow sp^+_{2,3/2}}$. Such phenomenon is the transient-absorption analog of the holographic principle in photoelectron spectra [45].

IV. BIDIMENSIONAL XUV SPECTROSCOPY

To interpret the ATAS spectrum more systematically, let us consider again Eq. (1). Since the XUV pulse is weak, the dipole response, at the response frequency ω_r, of the laser-driven system can be assumed to be linear in the XUV part of the spectrum of the impinging electric field,

$$\tilde{d}(\omega_r;\mathcal{E}) = \int d\omega_e \chi(\omega_r,\omega_e)\tilde{\mathcal{E}}(\omega_e), \tag{3}$$

where $\chi(\omega_r,\omega_e)$ is the electric susceptibility of the dressed atom and ω_e indicates a frequency at which the system is excited. For time-invariant samples, the susceptibility is diagonal, $\chi(\omega_r,\omega_e) = \delta(\omega_r - \omega_e)\chi_d(\omega_r)$. For ATAS, in contrast, $\chi(\omega_r,\omega_e)$ *is not* diagonal: under the action of any given excitation frequency, a dressed atom will respond at other frequencies as well. Thus, alongside the diagonal component, the electrical susceptibility also comprises a nondiagonal component χ_{nd},

$$\chi(\omega_r,\omega_e) = \delta(\omega_r - \omega_e)\chi_d(\omega_r) + \chi_{nd}(\omega_r,\omega_e). \tag{4}$$

For moderate intensities of the dressing laser, the strongest features of χ_{nd} are located close to the lines $\omega_r = \omega_e + 2n\omega_{VIS}$, with $n = 0, \pm1, \pm2, \ldots$. If the spectrum of the XUV pulse is narrower than $2\omega_{VIS}$, as in [20,46,47], transient absorption only probes the response close to the diagonal $\omega_r = \omega_e$. This provides valuable yet incomplete information on the ultrafast optical response of the dressed system. In ATAS, on the other hand, the spectral width of the attosecond pulse exceeds $2\omega_{VIS}$, therefore the off-diagonal response, e.g., at $\omega_r = \omega_e \pm 2\omega_{VIS}$, results in a detectable heterodyne signal. This result holds for isolated as well as for trains [4,48,49] of attosecond pulses. By combining Eqs. (1)–(4) and using the relationship

$$\tilde{\mathcal{E}}(\omega) = \tilde{\mathcal{E}}(\omega;\tau) = e^{-i\omega\tau}\tilde{\mathcal{E}}_0(\omega) \tag{5}$$

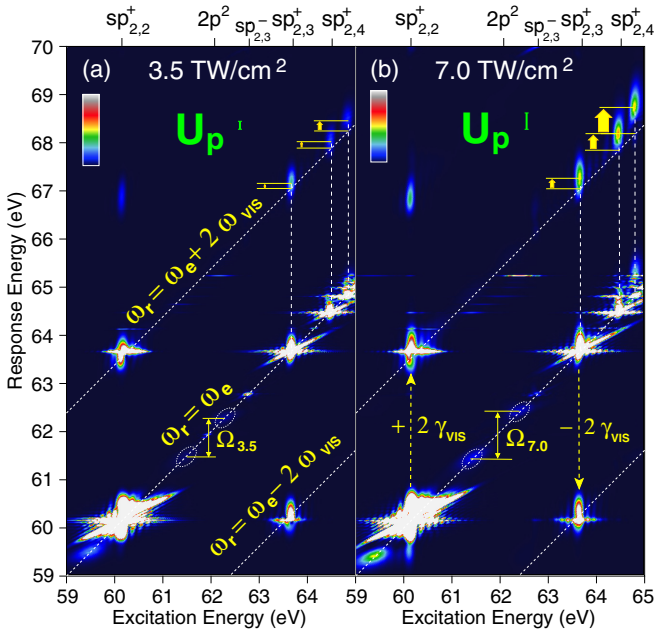

FIG. 3. (Color online) Square module of the FT of the effective absorption cross section $\tilde{\sigma}(\omega_r,|\omega_r - \omega_e|)$ as a function of the excitation (ω_e) and of the response energy (ω_r), for (a) $I_0 = 3.5$ TW/cm^2 and (b) $I_0 = 7$ TW/cm^2. In the spectral region examined here, apart for a multiplicative factor, this quantity is a good approximation to the squared modulus of the nondiagonal XUV electrical susceptibility $|\chi_{nd}(\omega_r,\omega_e)|^2$ of the dressed helium atom.

in the limit of an extremely short XUV pulse (for which $\tilde{\mathcal{E}}_0(\omega)$ is constant in the spectral range of interest), one can relate the FT of the ATAS spectrum,

$$\tilde{\sigma}(\omega_r,\omega_\tau) = \int_{-\infty}^{\infty} d\tau \frac{e^{-i\omega_\tau \tau}}{\sqrt{2\pi}}[\sigma(\omega_r,\tau) - \sigma(\omega_r,\infty)], \tag{6}$$

to the nondiagonal susceptibility $\chi_{nd}(\omega_r,\omega_e)$, obtaining

$$\tilde{\sigma}(\omega_r,\omega_\tau) = \frac{(2\pi)^{3/2}\omega_r}{ic}[\chi_{nd}(\omega_r,\omega_r - \omega_\tau) - \chi^*_{nd}(\omega_r,\omega_r + \omega_\tau)]. \tag{7}$$

In Fig. 3 we plot, for two different peak intensities of the dressing laser, $I_0 = 3.5$ TW/cm^2 and $I_0 = 7$ TW/cm^2, the squared module of $\tilde{\sigma}(\omega_r,\omega_\tau)$ for $\omega_\tau = |\omega_r - \omega_e|$, as a function of ω_r and ω_e, for an "excitation energy" $\hbar\omega_e$ in the range of the $sp^+_{2,n}$ series, and for a "response energy" $\hbar\omega_r$ up to $\simeq$5 eV above the $N = 2$ threshold. Due to the resonant structure of helium, in this range the second term on the right-hand side of Eq. (7) features only peaks along the $\omega_r = \omega_e$ diagonal that overlap to those already present in the first term. To discuss the location of the features of the nondiagonal susceptibility, $\chi_{nd}(\omega_r,\omega_e)$, therefore, we can simply look at those of $\tilde{\sigma}(\omega_r,|\omega_r - \omega_e|)$.

The strong signals close to the $\omega_r = \omega_e$ axis in Fig. 3 are associated to the induced transparency of the DES visible also in femtosecond TAS [20,23,27]. The two strong heterodyne signals at $(\omega_e,\omega_r) = (\omega_{sp^+_{2,2/3},g},\omega_{sp^+_{2,2/3},g} \pm 2\omega_{VIS})$, instead, are visible only if the individual pulses in the XUV field (which may be part of a train) have a duration smaller than

half the period of the dressing field. Along the diagonal, at $\omega_e = \omega_r = \omega_{2p^2,g} \pm \Omega/2$, we recognize the AT doublet of the $2p^2$ dressed ^1S resonance, and the increase with intensity of the Rabi frequency $\Omega(I_0)$ of the $2p^2 \leftarrow sp^+_{2,2}$ transition, which, in stationary conditions, is given by $\Omega_{st}(I_0) = \sqrt{\delta^2 + |\mu\mathcal{E}_0|^2}$, where the laser has a detuning $\delta = -0.237$ eV, and the dipole moment μ between the two DES is known from literature, $\mu_{sp^+_{2,2},2p^2} = 2.17$ a.u. [23]. The Rabi frequencies extracted from Fig. 3, $\Omega(3.5\ \mathrm{TW/cm^2}) = 0.80$ eV and $\Omega(7.0\ \mathrm{TW/cm^2}) = 0.98$ eV, qualitatively agree with those predicted by the stationary formula, $\Omega_{st}(3.5\ \mathrm{TW/cm^2}) = 0.64$ eV, $\Omega_{st}(7.0\ \mathrm{TW/cm^2}) = 0.87$ eV.

V. MULTIELECTRON ac STARK SHIFT

Looking again at Fig. 3, the two-photon-absorption signals from the $sp^+_{2,3-5}$ states are clearly shifted upward with respect to the $\omega_r = \omega_e + 2\omega_{VIS}$ line, due to the ac Stark shift experienced by these states. Notice that the stimulated two-photon emission signals at $\omega_e - 2\omega_{VIS}$ from the same states are not visible in the spectrum. This is because the radiative transition $sp^+_{2,4-5} \rightarrow 2\gamma_{VIS} + 1sE_\ell$ is suppressed in the independent-particle limit, while the two-photon absorption to the $N = 2$ channels, $sp^+_{2,4-5} + 2\gamma_{VIS} \rightarrow 2s/2pE_\ell$, is active. In contrast to what is known for the singly-excited states in helium [33], the ac Stark shift for the highest terms of the autoionizing $sp^+_{2,n}$ series significantly exceeds the ponderomotive energy $U_p = \mathcal{E}_0^2/4\omega^2_{VIS}$, which is the limiting value expected for a Rydberg electron bound to an unpolarizable core [50]. This finding indicates that the correlated Rydberg and core electrons give comparable contributions to the polarization of the state, which is a clear-cut confirmation of the multielectron character of the atomic response to intense external fields evidenced in previous studies on tunneling suppression [29,30].

In Fig. 4(a) we show the dependence of the ATAS on the intensity of the dressing laser at a fixed time delay $\tau = 200$ as. We observe an increase of the AT splitting of the $sp^+_{2,2}$ resonance with intensity, as well as the branches of the $2p^2$ dressed state. An inversion of the Fano profile for all the higher terms in the $sp^+_{2,n}$ series is also clearly visible as the intensity of the dressing field increases. In [17], this latter effect has been attributed to the ac Stark shift $\Delta E^{ac}_i(t)$ of the autoionizing states, which translates into an extra phase $\Delta\phi_i(I_0) = -\int_{-\tau}^{\infty} \Delta E^{ac}_i[I(t)]dt$ between resonant and background amplitudes, a quantity approximately proportional to the peak intensity I_0 of the laser [51]. In principle, therefore, the inversion of the Fano profiles should take place multiple times as the laser intensity increases. Our calculations confirm such repeated inversion [see Fig. 4(b)].

From the Fano profiles of the $sp^+_{2,3-6}$ and $sp^-_{2,5}$ states, $\sigma_i(\omega, I_0) \sim \sigma_{0,i}(I_0) + \frac{[\epsilon_i + q_i(I_0)]^2}{1+\epsilon_i^2}$, where $\epsilon_i = 2(\omega - \omega_{i,g})/\Gamma_i$ is the reduced energy with respect to each resonance, we extract the q parameters. The intensity-dependent phase of the states, $\varphi_i(I_0)$, is then obtained as $\varphi_i(I_0) = -2\arctan q_i(I_0)$ [17]. The variation of such phase, $\Delta\varphi_i(I_0) = \varphi_i(I_0) - \varphi(0)$, is finally compared to the phase shift expected for a Rydberg singly excited state: $\Delta\varphi_{free} = \hbar^{-1}\int_{-\tau}^{\infty} U_p[I(t)]dt$. Figure 4(c) shows that the ratio $\Delta\varphi_i(I_0)/\Delta\varphi_{free}(I_0)$ differs strikingly from unity,

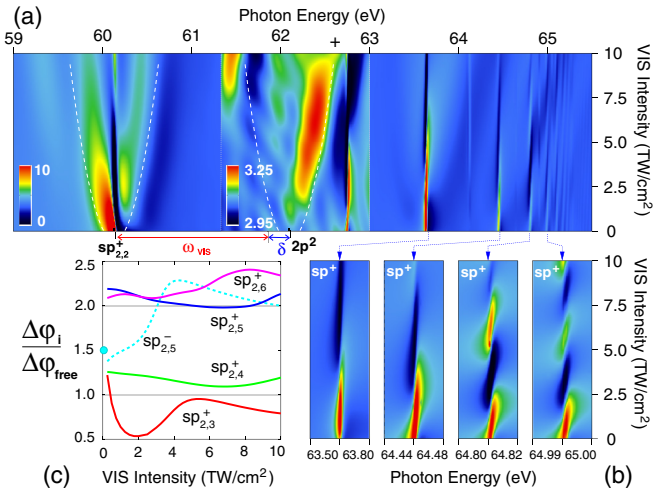

FIG. 4. (Color online) (a) ATAS spectrum for overlapping XUV and VIS pulses as a function of the XUV photon energy (x axis) and of the intensity of the VIS dressing field (y axis); to highlight the AT splitting of the $2p^2$ state, the spectrum between 61.3 and 63 eV is shown with enhanced color contrast. The dashed white lines indicate the peak splitting for the stationary detuned Rabi flopping with $\Omega(I) = \sqrt{\delta^2 + |\mu\mathcal{E}_0|^2}$. (b) details of the spectrum near the $sp^+_{2,3-6}$ DES, whose Fano profiles undergo several inversions as the intensity of the dressing laser increases. (c) DES phase compared to the SAE Rydberg limit.

which is the expected value for a Rydberg singly excited state. Apart from the $sp^+_{2,3}$ state, the phase ratios lie well above unity, reaching values twice as large for $n \geqslant 5$. Furthermore, even if the phase increases monotonically with the laser intensity, the phase ratio is clearly structured. In the case of the $sp^+_{2,3}$ state, the intensity dependence may be due to a detuned Rabi oscillation with the $[sp^+_{2,2} - 2p^2]$ pair. For the other states, the modulation arises from multiple concurrent coupling mechanisms, including coupling with other autoionizing states, as well as with states in the continuum above the $N = 2$ threshold. For the narrow $sp^-_{2,5}$ state, we made a perturbative estimate of the polarizability, finding a value that is consistent with the change of phase observed for $I_0 \simeq 0$. The ac Stark shift ΔE^{ac} of the $sp^-_{2,5}$ state was computed with the well-known second-order perturbative formula, adapted to autoionizing states,

$$\Delta E^{ac}_i(\omega_{VIS}) = -\frac{F_0^2}{2}\sum_j \frac{\langle\varphi^L_i|P|\varphi^R_j\rangle\langle\varphi^L_j|P|\varphi^R_i\rangle}{\omega_{ij}(\omega^2_{ij} - \omega^2_{VIS})}, \qquad (8)$$

where F_0 is the electric field amplitude, P is the total electronic canonical momentum operator, $\langle\varphi^L_i|H'_0 = E_i\langle\varphi^L_i|$ and $H'_0|\varphi^R_i\rangle = |\varphi^R_i\rangle E_i$ are the left and right eigenvectors, respectively, of a non-Hermitian reference Hamiltonian H'_0, the E_i are the corresponding complex eigenvalues, and $\omega_{ij} = E_i - E_j$. The operator H'_0 is defined as the field-free Hamiltonian of the atom plus a complex absorption potential (CAP) $V = v(r_1) + v(r_2)$, $v(r) = -i\eta(r - R_0)^2\theta(r - R_0)$, which enforces outgoing boundary conditions. The real positive parameter η is varied until the expression for the ac Stark shift approaches an almost stationary value [52]. In contrast to what is observed when the reference Hamiltonian is regularized using exterior complex scaling (ECS) [53,54]

instead of CAPs, due to the alteration of the wave functions in the complex-absorption region, the continuum-continuum matrix elements in Eq. (8) attain reasonably stationary values only for the narrowest resonances. We have ascertained that our estimates are reasonably converged by benchmarking them against selected ECS accurate calculations [55].

VI. CONCLUSIONS

In conclusion, we have shown that ATAS allows one to measure the nonperturbative response of autoionizing states to external dressing fields. In particular, the AT splitting of the dressed $2p^2\,{}^1S$ dark state can be measured, and the inversion of asymmetric resonant features in the spectrum is found to repeat almost periodically as the intensity of the driving laser is increased. The ac Stark shift of the doubly excited states, which are important parameters for the implementation of quantum-control protocols, are shown to increase nonlinearly with the intensity of the dressing field and, for the higher states of the autoionizing $sp^+_{2,n}$ series, to exceed by more than twice the theoretical SAE limit. These results confirm once again the failure of the SAE approximation in describing ionization from strongly correlated multielectron states. Finally, we have established a relationship between the ATAS spectra and the nondiagonal components of the XUV electrical susceptibility, thus extending multidimensional spectroscopy to the XUV domain, which provides an alternative way to measure shifts of and coherences between states above the ionization threshold.

ACKNOWLEDGMENTS

We thank Andrej Mihelič for providing us benchmark values for the polarizability of some doubly excited states, which were useful to validate our own perturbative approach to calculation of this quantity. We acknowledge computer time from the CCC-UAM and Marenostrum Supercomputer Centers and financial support from the European Research Council under the European Union's Seventh Framework Programme (FP7/2007-2013)/ERC grant agreement 290853 XCHEM, the MINECO project FIS2013-42002-R, the ERA-Chemistry Project PIM2010EEC-00751, the European COST Action XLIC CM1204, the Marie Curie ITN CORINF, and the CAM project NANOFRONTMAG. C.O. and T.P. acknowledge financial support by the Max-Planck Research Group Program of the Max-Planck Gesellschaft (MPG) and the European Research Council (ERC, Grant No. X-MuSiC-616783).

[1] M. Chini, K. Zhao, and Z. Chang, Nat. Photonics **8**, 178 (2014).
[2] E. Goulielmakis, Z.-H. Loh, A. Wirth, R. Santra, N. Rohringer, V. S. Yakovlev, S. Zherebtsov, T. Pfeifer, A. M. Azzeer, M. F. Kling *et al.*, Nature (London) **466**, 739 (2010).
[3] H. Wang, M. Chini, S. Chen, C.-h. Zhang, Y. Cheng, F. He, Y. Wu, U. Thumm, and Z. Chang, Phys. Rev. Lett. **105**, 143002 (2010).
[4] M. Holler, F. Schapper, L. Gallmann, and U. Keller, Phys. Rev. Lett. **106**, 123601 (2011).
[5] C. Ott, A. Kaldun, L. Argenti, P. Raith, K. Meyer, M. Laux, Y. Zhang, A. Blättermann, S. Hagstotz, T. Ding *et al.*, Nature (London) **516**, 374 (2014).
[6] A. R. Beck, B. Bernhardt, E. R. Warrick, M. Wu, S. Chen, M. B. Gaarde, K. J. Schafer, D. M. Neumark, and S. R. Leone, New J. Phys. **16**, 113016 (2014).
[7] E. Heinrich-Josties, S. Pabst, and R. Santra, Phys. Rev. A **89**, 043415 (2014).
[8] A. Wirth, M. T. Hassan, I. Grguras, J. Gagnon, A. Moulet, T. T. Luu, S. Pabst, R. Santra, Z. A. Alahmed, A. M. Azzeer *et al.*, Science **334**, 195 (2011).
[9] X. Wang, M. Chini, Y. Cheng, Y. Wu, X. M. Tong, and Z. Chang, Phys. Rev. A **87**, 063413 (2013).
[10] S. Chen, M. J. Bell, A. R. Beck, H. Mashiko, M. Wu, A. N. Pfeiffer, M. B. Gaarde, D. M. Neumark, S. R. Leone, and K. J. Schafer, Phys. Rev. A **86**, 063408 (2012).
[11] S. Chen, M. Wu, M. B. Gaarde, and K. J. Schafer, Phys. Rev. A **87**, 033408 (2013).
[12] S. Chen, M. Wu, M. B. Gaarde, and K. J. Schafer, Phys. Rev. A **88**, 033409 (2013).
[13] J. Herrmann, M. Weger, R. Locher, M. Sabbar, P. Rivière, U. Saalmann, J.-M. Rost, L. Gallmann, and U. Keller, Phys. Rev. A **88**, 043843 (2013).
[14] M. Chini, X. Wang, Y. Cheng, and Z. Chang, J. Phys. B: At., Mol. Opt. Phys. **47**, 124009 (2014).
[15] J. Ullrich, R. Moshammer, A. Dorn, R. Dörner, L. P. H. Schmidt, and H. Schmidt-Böcking, Rep. Prog. Phys. **66**, 1463 (2003).
[16] A. T. J. B. Eppink and D. H. Parker, Rev. Sci. Instrum. **68**, 3477 (1997).
[17] C. Ott, A. Kaldun, P. Raith, K. Meyer, M. Laux, J. Evers, C. H. Keitel, C. H. Greene, and T. Pfeifer, Science **340**, 716 (2013).
[18] A. Blättermann, C. Ott, A. Kaldun, T. Ding, and T. Pfeifer, J. Phys. B: At., Mol. Opt. Phys. **47**, 124008 (2014).
[19] A. Kaldun, C. Ott, A. Blättermann, M. Laux, K. Meyer, T. Ding, A. Fischer, and T. Pfeifer, Phys. Rev. Lett. **112**, 103001 (2014).
[20] M. B. Gaarde, C. Buth, J. L. Tate, and K. J. Schafer, Phys. Rev. A **83**, 013419 (2011).
[21] M. V. Ammosov, N. B. Delone, and V. P. Krainov, J. Exp. Theor. Phys. **91**, 2008 (1986).
[22] A. M. Perelomov, V. S. Popov, and M. V. Terent'ev, J. Exp. Theor. Phys. **23**, 924 (1966).
[23] Z.-H. Loh, C. H. Greene, and S. R. Leone, Chem. Phys. **350**, 7 (2008).
[24] S. I. Themelis, P. Lambropoulos, and M. Meyer, J. Phys. B: At., Mol. Opt. Phys. **37**, 4281 (2004).
[25] W.-C. Chu, S.-F. Zhao, and C. D. Lin, Phys. Rev. A **84**, 033426 (2011).
[26] W.-C. Chu and C. D. Lin, Phys. Rev. A **85**, 013409 (2012).
[27] W.-C. Chu and C. D. Lin, J. Phys. B: At., Mol. Opt. Phys. **45**, 201002 (2012).
[28] M. Chini, B. Zhao, H. Wang, Y. Cheng, S. X. Hu, and Z. Chang, Phys. Rev. Lett. **109**, 073601 (2012).
[29] M. Smits, C. A. de Lange, A. Stolow, and D. M. Rayner, Phys. Rev. Lett. **93**, 203402 (2004).

[30] A. N. Pfeiffer, C. Cirelli, M. Smolarski, D. Dimitrovski, M. Abu-samha, L. B. Madsen, and U. Keller, Nat. Phys. **8**, 76 (2011).
[31] P. Lambropoulos and P. Zoller, Phys. Rev. A **24**, 379 (1981).
[32] H. Bachau, P. Lambropoulos, and R. Shakeshaft, Phys. Rev. A **34**, 4785 (1986).
[33] X. M. Tong and N. Toshima, Phys. Rev. A **81**, 063403 (2010).
[34] L. Argenti and E. Lindroth, Phys. Rev. Lett. **105**, 053002 (2010).
[35] A. Jiménez-Galán, L. Argenti, and F. Martín, Phys. Rev. Lett. **113**, 263001 (2014).
[36] D. A. Varshalovich, A. N. Moskalev, and V. K. Kersonskii, *Quantum Theory of Angular Momentum* (World Scientific, Singapore, 1984).
[37] L. Argenti and R. Moccia, J. Phys. B: At., Mol. Opt. Phys. **39**, 2773 (2006).
[38] S. Balay, S. Abhyankar, M. F. Adams, J. Brown, P. Brune, K. Buschelman, V. Eijkhout, W. D. Gropp, D. Kaushik, M. G. Knepley *et al.*, PETSc Web page, http://www.mcs.anl.gov/petsc (2014).
[39] S. Balay, S. Abhyankar, M. F. Adams, J. Brown, P. Brune, K. Buschelman, V. Eijkhout, W. D. Gropp, D. Kaushik, M. G. Knepley *et al.*, Argonne National Laboratory, Technical Report No. ANL-95/11 - Revision 3.5, 2014 (unpublished), http://www.mcs.anl.gov/petsc.
[40] S. Balay, W. D. Gropp, L. C. McInnes, and B. F. Smith, in *Modern Software Tools in Scientific Computing*, edited by E. Arge, A. M. Bruaset, and H. P. Langtangen (Birkhäuser Press, Boston, 1997), pp. 163–202.
[41] J. Cooper, U. Fano, and F. Prats, Phys. Rev. Lett. **10**, 518 (1963).
[42] U. Fano, Phys. Rev. **124**, 1866 (1961).
[43] R. Madden and K. Codling, Phys. Rev. Lett. **10**, 516 (1963).
[44] L. Argenti, R. Pazourek, J. Feist, S. Nagele, M. Liertzer, E. Persson, J. Burgdörfer, and E. Lindroth, Phys. Rev. A **87**, 053405 (2013).
[45] J. Mauritsson, T. Remetter, M. Swoboda, K. Klünder, A. L'Huillier, K. J. Schafer, O. Ghafur, F. Kelkensberg, W. Siu, P. Johnsson *et al.*, Phys. Rev. Lett. **105**, 053001 (2010).
[46] C. Buth, R. Santra, and L. Young, Phys. Rev. Lett. **98**, 253001 (2007).
[47] C. Buth and R. Santra, Phys. Rev. A **78**, 043409 (2008).
[48] P. Ranitovic, X. M. Tong, C. W. Hogle, X. Zhou, Y. Liu, N. Toshima, M. M. Murnane, and H. C. Kapteyn, Phys. Rev. Lett. **106**, 193008 (2011).
[49] N. Shivaram, H. Timmers, X. M. Tong, and A. Sandhu, Phys. Rev. Lett. **108**, 193002 (2012).
[50] M. D. Davidson, J. Wals, H. G. Muller, and H. B. van Linden van den Heuvell, Phys. Rev. Lett. **71**, 2192 (1993).
[51] C. Marante, L. Argenti, and F. Martín, Phys. Rev. A **90**, 012506 (2014).
[52] R. Santra, Phys. Rev. A **74**, 034701 (2006).
[53] A. Mihelič and M. Žitnik, Phys. Rev. Lett. **98**, 243002 (2007).
[54] M. Žitnik, A. Mihelič, K. Bučar, M. Kavčič, J.-E. Rubensson, M. Svanquist, J. Söderström, R. Feifel, C. Såthe, Y. Ovcharenko *et al.*, Phys. Rev. Lett. **113**, 193201 (2014).
[55] A. Mihelič (private communication).